



3D geodynamic models for the development of opposing continental subduction zones: The Hindu Kush–Pamir example



Jie Liao^{a,*}, Taras Gerya^a, Marcel Thielmann^b, A. Alexander G. Webb^c,
Sofia-Katerina Kufner^d, An Yin^e

^a Geophysical Fluid Dynamics, Institute of Geophysics, ETH Zurich, Sonneggstrasse 5, CH-8092, Zurich, Switzerland

^b Bayerisches Geoinstitut, University of Bayreuth, Universitätsstraße 30, 95440 Bayreuth, Germany

^c Department of Earth Sciences and Laboratory of Space Research, University of Hong Kong, Hong Kong, China

^d Deutsches GeoForschungsZentrum GFZ, Telegrafenberg, 14473 Potsdam, Germany

^e Department of Earth, Planetary, and Space Sciences, University of California, Los Angeles, CA 90095-1567, USA

ARTICLE INFO

Article history:

Received 22 May 2017

Received in revised form 1 October 2017

Accepted 4 October 2017

Available online 2 November 2017

Editor: P. Shearer

Keywords:

continental subduction zones

opposite subduction polarities

Hindu Kush–Pamir orogenic system

3D geodynamic model

ABSTRACT

The development of opposing continental subduction zones remains scantily explored in three dimensions. The Hindu Kush–Pamir orogenic system at the western end of the Himalayan orogen provides a rare example of continental collision linked to two opposing intra-continental subduction zones. The subducted plates feature a peculiar 3D geometry consisting of two distinct lithospheric fragments with different polarities, subduction angles and slab-curvatures beneath the Hindu Kush and Pamir, respectively. Using 3D geodynamic modeling, we simulate possible development of two opposing continental subduction zones to understand the dynamic evolution of the Hindu Kush–Pamir orogenic system. Our geodynamic model reproduces the major tectonic elements observed: (1) the deeper subduction depth, the steeper dip angle and the southward offset of the Hindu Kush subduction zone relative to the Pamir naturally occur if convergence direction of the subducting Indian plate and dip-direction of the Hindu Kush subduction zone match. (2) The formation of the highly asymmetrically curved Pamir region and the south-dipping subduction is promoted by the initial geometry of the indenting Indian lithosphere together with the existence of a major strike-slip fault on the eastern margin of the Pamir region. (3) Subduction of only the lower continental crust during continental collision can occur if the coupling between upper and lower crusts is weak enough to allow a separation of these two components, and that (4) the subduction of mainly lower crust then facilitates that conditions for intermediate-depth seismicity can be reached. (5) The secondary tectonic features modeled here such as strike-slip-fault growth, north–northwest striking extension zone, and lateral flow of the thickened ductile upper crust are comparable to the current tectonics of the region. (6) Model results are further compared to the potentially similar orogenic system, i.e., the Alpine orogen, in terms of the curved Western Alpine arc and the two opposing subducted slabs beneath the Alps and the Dinarides.

© 2017 Elsevier B.V. All rights reserved.

1. Introduction

Recent three-dimensional numerical modeling studies indicate that the interaction of subducting slabs across two opposing subduction zones can promote the formation of curved mountain belts, and severely influence the subsequent dynamics of these orogenic systems (Király et al., 2016). At the same time, true observations of intervening continental slabs are sparse as the time between slab interaction and break-off is ephemeral

(Kufner et al., 2017). Among a range of observational and modeling approaches, quantitative understanding of continental collision dynamics may be gained via two-dimensional numerical modeling (e.g., Beaumont et al., 2001; Faccenda et al., 2008; Yamato et al., 2008; Li et al., 2011; Vogt and Gerya, 2014; Liao and Gerya, 2017). In such models, quasi-infinite homogeneity is assumed in the third dimension. Three dimensional numerical studies of continental collision are limited, but are essential in investigating key aspects of realistic, three-dimensional orogenic systems, in particular the controls of lateral heterogeneities on collisional dynamics (e.g., van Hunen and Allen, 2011; Li et al., 2013; Capitanio, 2014; Moresi et al., 2014; Pusok and Kaus, 2015; Chen and Gerya, 2016; Menant et al., 2016). Thus far, such 3D models have mainly focused on the

* Corresponding author.

E-mail address: jie.liao@erdw.ethz.ch (J. Liao).

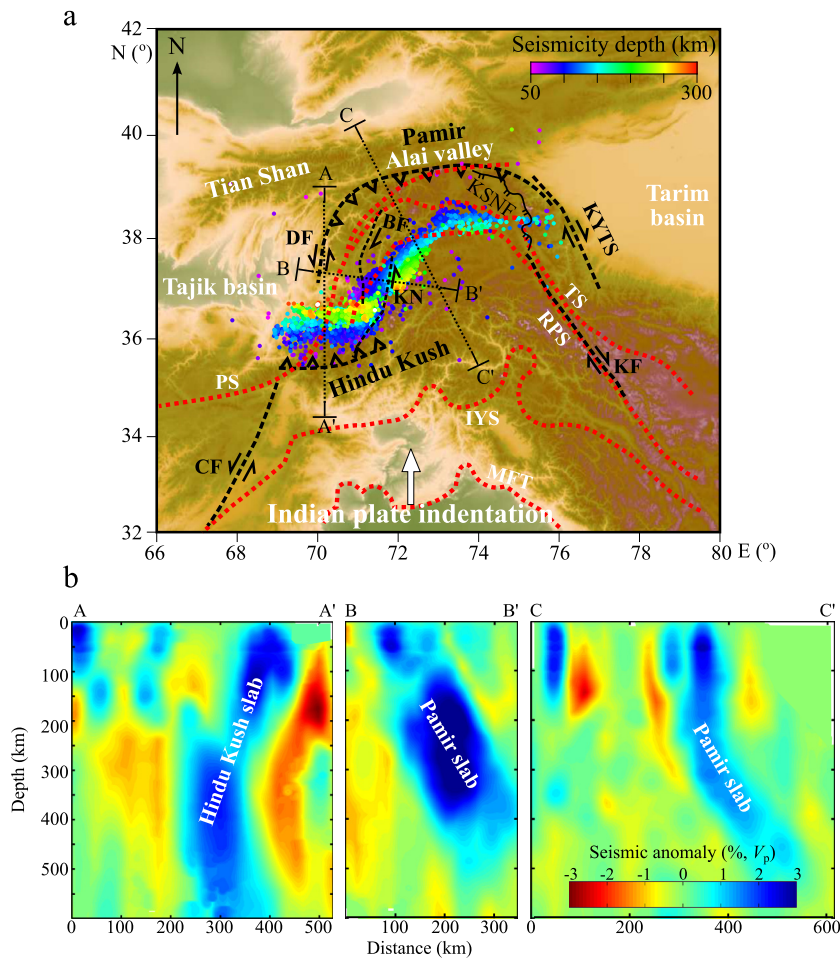


Fig. 1. Tectonic setting of the Hindu Kush–Pamir orogenic system. (a) Simplified major sutures and strike-slip faults shown on a topography basemap. Black dashed lines with teeth mark the Hindu Kush and Pamir subduction zones. Black dashed lines with abbreviations represent strike-slip faults: CF: Chaman fault, DF: Darvaz fault, BF: Badakhshan fault, KN: Kapisā–Nuristan fault, KYTS: Kashgar Yecheng transfer system, KF: Karakorum fault. Suture zones are marked by red dotted lines: PS: Paleozoic suture, IYS: Indus–Yarlung suture, MFT: Main Frontal Thrust, RPS: Rushan–Pshart suture, TS: Tanyamas suture. The east–west extensional Kongur Shan normal fault (KSNF) is marked. Seismic events deeper than 50 km (Kufner et al., 2016) are projected on the surface. (b) Seismic profiles across the Hindu Kush–Pamir region (Kufner et al., 2016). Sutures and faults are drawn based on Kufner (2016), Sobel et al. (2013), and Burtman and Molnar (1993). (For interpretation of the references to color in this figure legend, the reader is referred to the web version of this article.)

influence/control of oceanic subduction on the juxtaposed continental collision in settings where the imposed oceanic subduction and continental collision share the same polarity. In contrast, the dynamic evolution of continental subductions with opposite polarities is rarely addressed, and has been scantily investigated through 3D geodynamic models.

The Hindu Kush–Pamir orogenic system at the northwestern end of the Himalayan orogen offers a rare opportunity to explore the development of two opposing continental subduction zones. This orogenic system hosts several striking tectonic features (Fig. 1). (1) Two opposite dipping slabs exist beneath the Hindu Kush and Pamir, exhibiting contrasting 3D geometry although being located directly next to each other: north-dipping slab of Indian origin beneath the Hindu Kush; south-dipping slab of Asian origin beneath the Pamir (Figs. 1a and b, Burtman and Molnar, 1993; Negrodo et al., 2007; Sippl et al., 2013; Kufner et al., 2016). The two subduction zones are dramatically different in terms of slab steepness and subduction depth: the Hindu Kush subducted slab in the south is much steeper ($\sim 80^\circ$) and deeper (> 500 km) than the Pamir slab ($\sim 45^\circ$ and > 300 km) in the north (Fig. 1b, Negrodo et al., 2007; Kufner et al., 2016). (2) Further, the Pamir orogen is offset several hundred kilometers north relative to its surroundings (e.g., 300 km, Burtman and Molnar, 1993). It therefore presents a highly arcuate but asymmetric geometry in map view (Fig. 1a). The eastern Pamir margin is marked by large

relatively straight strike-slip systems (e.g., the Kashgar–Yecheng transfer system and Karakorum Fault; Cowgill, 2010; Sobel et al., 2013), whereas the east–west striking Hindu Kush seismic zone is far less curved (Fig. 1a). (3) Lastly, numerous intermediate-depth earthquakes (at depths between 50 and 300 km) occur during the continental subduction (e.g., Sippl et al., 2013; Kufner et al., 2016). The reasons causing this seismicity remain enigmatic, since brittle failure is unlikely to occur due to high confining pressures. Several possible mechanisms have been proposed to result in intermediate-depth earthquakes, with the two mainly favored mechanisms being dehydration embrittlement (e.g., Kirby et al., 1996; Hacker et al., 2003) and thermal runaway (e.g., Kelemen and Hirth, 2007; John et al., 2009; Thielmann et al., 2015).

To what extent is this unique orogenic system idiosyncratic, and to what extent does it provide a snapshot of processes that may be more broadly experienced by orogenic systems? Complex slab interactions such as those observed across the Hindu Kush–Pamir orogenic system may be relatively ephemeral, and yet mark key turning points in orogenic evolution (e.g., Kufner et al., 2016; Webb et al., 2017). As such, inferring the dynamic evolution of the two opposing continental subduction zones may be fundamental to deciphering the development and interaction of many orogenic systems. Therefore in this study, we offer the first 3D geodynamic model of the Hindu Kush–Pamir orogenic system in order to simulate the processes responsible for generating the first-

order regional tectonic framework. We keep our model geometry close enough to the Hindu Kush–Pamir setting in order to ‘ground truth’ our model against nature but as simple as possible at the same time in order to most effectively discriminate between the competing effects of different model parameters on the development of the region and continental subduction zones in general. Our findings reveal how key crustal and mantle controls led to the formation of the Hindu Kush–Pamir curved orogenic system with opposing continental subduction and corresponding seismic zonation. We then compare these findings to another potentially similar orogenic systems, i.e., the Alpine orogen.

2. Geologic setting

This continental subduction beneath Hindu Kush and Pamir cannot be driven primarily by a precursor long-lasting oceanic subduction, since the Indian oceanic subduction terminated no later than 40 Ma along the Indus–Yarlung suture (Yin and Harrison, 2000; Tapponnier et al., 2001), and so far no remnants of a land-locked oceanic basin have been identified (Burtman and Molnar, 1993). Therefore, the deep subduction of continental lithosphere beneath Hindu Kush and Pamir is a rare case in nature since thick and buoyant continental lithosphere (e.g., crustal thickness of 35 km or more) was proposed to resist subduction (e.g., Molnar and Gray, 1979).

The Hindu Kush–Pamir orogenic system occupies the narrowest part of the Himalaya–Tibetan orogen (Yin and Harrison, 2000). Tectonic evolution of the Hindu Kush–Pamir region since the Paleozoic is characterized by intense north–south shortening (>600 km) and the successive accretion of different terranes (Burtman and Molnar, 1993; Negrodo et al., 2007; Sobel et al., 2013). Multiple Paleozoic to Cenozoic thrusts/suture zones developed, including the Mesozoic Tanymas and Rushan–Pshart sutures that divide the Pamir region into the North, Central and South Pamir. Contemporary and after the aggregation of these terranes, different major strike-slip faults formed and offset the Pamir north relative to the Hindu Kush (e.g., Burtman and Molnar, 1993; Schurr et al., 2014).

The Pamir region is surrounded by the Tarim basin in the east, the Tian Shan orogen and the Alai valley in the north and the Tajik basin in the west. The Alai valley is a relic of the previously connected Tajik and Tarim basins which were separated due to the northward indentation (>300 km) of the Main Pamir Thrust along the northern edge of the Pamir region (Burtman and Molnar, 1993). The Main Pamir Thrust represents the active northward retreating continental subduction zone (Sobel et al., 2013). More than 600 km convergence occurred between the southern Tian Shan and the southern Pamir in the Pamir region (Burtman and Molnar, 1993); ~300 km of this convergence was accommodated by the southward subduction along the Main Pamir Thrust. The rest was intra-continental shortening mainly occurred in the Central and South Pamir (Burtman and Molnar, 1993).

Although some debate exists on the exact timing, the northward indentation of the Pamir presumably started at ~25–16 Ma (Sobel and Dumitru, 1997). Two end-member kinematic models were proposed to explain the present day highly arcuate shape of the Pamir region: (1) vertical-axis rotational radial thrusting and (2) non-rotational indentation bounded by conjugate strike-slip faults. Currently, the most likely model is a combination of those (Cowgill, 2010, and reference therein): i.e., rotational radial thrusting along the western margin and strike-slip movement (~280 km) along the pre-existing Kashgar–Yecheng transfer system (KYTS) to the east. By contrast, non-rotational indentation presumably occurred during the northward migration of the south Pamir, which is bounded by the Chaman fault to the west and the Karakorum fault to the east (Cowgill, 2010). Active east–west extension initiating at ~9 Ma was observed along the north–

northwest striking Kongur Shan extensional system at the north-eastern margin of the Pamir region (Robinson et al., 2004, 2007). The largest magnitude of extension occurs along the Kongur Shan massif in the middle portion of the Kongur Shan normal fault (Robinson et al., 2007). Several kinematic models have been proposed to explain the formation of the Kongur Shan extension system, with the currently preferred model of radial thrusting and oroclinal bending (Robinson et al., 2004, 2007). However, in order to explain the largest extension along the Kongur Shan massif, the synorogenic extension model (synchronous development of frontal thrusting and rear normal faulting along the Main Pamir Thrust) seems to be more likely.

The Hindu Kush forms to the southwest of the Pamir and results from the northward subduction of the Indian lithosphere although no surface outcrop of the major thrust along which subduction occurred could be identified (Burtman and Molnar, 1993). In contrast to the Pamir, which is restricted to the north by the Paleozoic suture, the Hindu Kush mountains contain this suture in their center. The other suture zones which were documented in the Pamir further south can also be traced into the Hindu Kush (e.g., Burtman and Molnar, 1993) but are less well described due to the currently difficult accessibility of the region. To the west, the Hindu Kush is restricted by the Chaman fault, which represents the western termination of the Indian Indenter.

3. Method

3.1. Numerical method

The 3D thermomechanical coupled numerical code I3ELVIS (Gerya, 2013) based on finite-differences and marker-in-cell techniques is used to solve the mass, momentum and energy conservation equations in a fully staggered grid assuming an incompressible medium:

$$\frac{\partial v_i}{\partial x_i} = 0 \quad (1)$$

$$\frac{\partial \sigma'_{ij}}{\partial x_j} - \frac{\partial P_i}{\partial x_i} = -\rho g_i \quad (2)$$

$$\rho C_p \frac{DT}{Dt} = \frac{\partial}{\partial x_i} \left(k \frac{\partial T}{\partial x_i} \right) + H_s + H_a + H_r + H_L \quad (3)$$

where v is velocity, σ' the deviatoric stress tensor, P the total pressure (mean normal stress), ρ density, g gravitational acceleration, C_p heat capacity, T temperature, k thermal conductivity, H internal heating, H_s shear heating ($H_s = \sigma'_{ij} \dot{\epsilon}_{ij}$, $\dot{\epsilon}$ strain rate tensor), H_a adiabatic heating ($H_a = T \alpha \frac{DP}{Dt}$, α thermal expansivity), H_r radioactive heating with a constant value for each rock, and H_L latent heating included implicitly by increasing the effective heat capacity and thermal expansion of the partially crystallized/molten rocks (Burg and Gerya, 2005). The Einstein notation is used for the indexes i and j , which denote spatial directions $i = (x, y, z)$ and $j = (x, y, z)$ in 3D. The multigrid method is used to speed up the convergence of the Gauss–Seidel iterations for the coupled solve of Eq. (1) and Eq. (2).

In our models, we employ a visco-plastic rheology. The non-Newtonian viscous rheology is strain rate-, pressure- and temperature-dependent. Plastic rheology is described by a Drucker–Prager yield criterion, where the yield stress (σ_y) is pressure dependent (C is rock cohesion and μ is the effective friction coefficient). Viscosity due to plastic deformation (η_{plas}) is computed based on the square root of the second invariant of strain rate ($\dot{\epsilon}_{II}$). Eventually, the effective viscosity of rocks (η_{eff}) is constrained by both viscous and plastic deformation. See further explanation of variables/symbols in Tables S1 and S2 in the supplement.

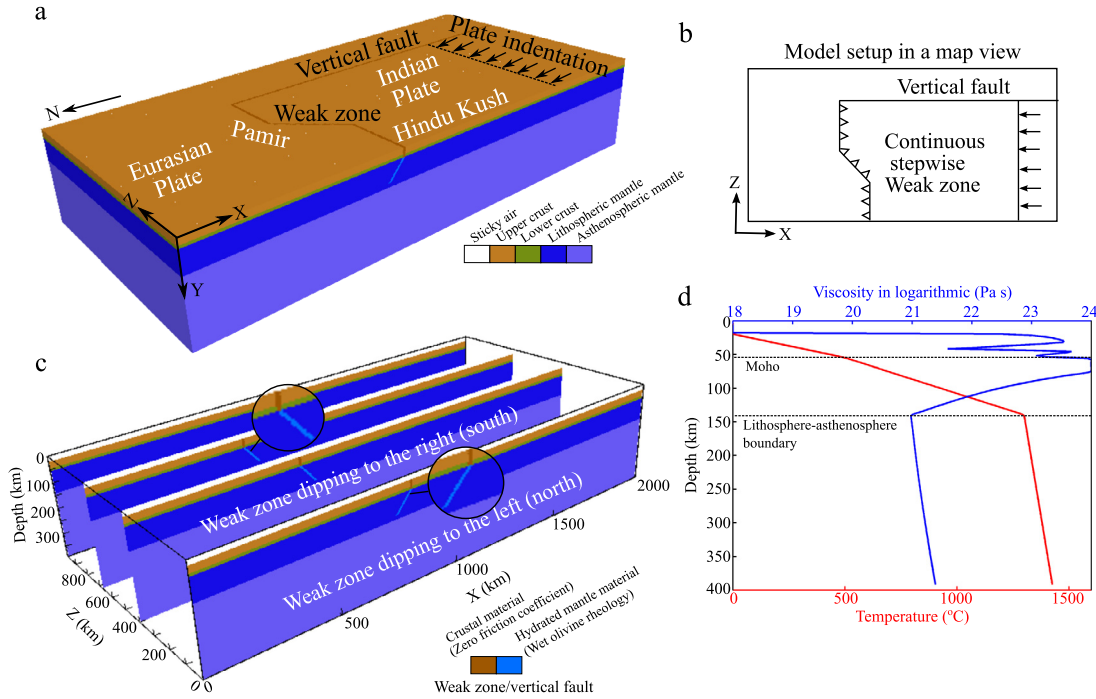


Fig. 2. Initial setup of the reference model. (a) Entire model domain color coded by lithology. Two continental plates are prescribed (the Eurasian plate on the left/north and the Indian Plate on the right/south). One vertical fault is prescribed on the right (east) of the Indian plate. A continuous weak zone is imposed to trigger collision/subduction between the Asian and Indian plate. In the Pamir region, the weak zone is split into two segments ('continuous stepwise zone'). (b) Map view showing the opposite polarities of the weak zone in the Hindu Kush and Pamir region, respectively. (c) Cross sections showing lithology and the opposite polarities of the weak zone in the Hindu Kush–Pamir region. (d) 1D initial temperature and viscosity profiles at $t = 5.1 \times 10^{-5}$ Ma. The entire model box is homogeneous except the weak zone and the vertical fault. Rock rheology is listed in Table S1.

$$\eta_{\text{vis}} = \frac{1}{2} A \frac{1}{n} \dot{\epsilon}_{\text{II}}^{\frac{1-n}{n}} \exp\left(\frac{PV_a + E_a}{nRT}\right) \quad (4)$$

$$\sigma_y = C + P\mu \quad (5)$$

$$\eta_{\text{plas}} = \frac{\sigma_y}{2\dot{\epsilon}_{\text{II}}} \quad (6)$$

$$\eta_{\text{eff}} = \min(\eta_{\text{vis}}, \eta_{\text{plas}}) \quad (7)$$

Sedimentation and erosion processes are implemented in a simplified way. During model development and the related crustal surface deformation, transmutation of sticky air markers into sticky water occurs when these markers move below the prescribed water level (i.e. 5 km below the initial crustal surface). Further transmutation of water markers into sediments occurs below the prescribed sedimentation level (i.e. 10 km below the initial crustal surface). Instantaneous erosion is prescribed at 10 km above the initial crustal level by converting rock markers into sticky air.

3.2. Model setup

The initial configuration of the reference 3D numerical model is shown in Fig. 2. The numerical model box contains 501 (X-axis: north–south) by 197 (Y-axis: depth) by 245 (Z-axis: west–east) uniformly distributed nodes, which corresponds to a physical dimension of 2000 km by 392 km by 976 km. Two continental plates are imposed in the model, i.e., the Eurasian plate on the left (north) and the Indian plates on the right (south). Northward indentation of the Indian plate drives collisional tectonics of this region (e.g., Replumaz et al., 2016). A marginal vertical fault (10 km wide and 105 km high) is prescribed to the right (east) of the Indian plate to facilitate future strike slipping. To facilitate subduction initiation, a weak zone is prescribed at the interface between both plates. In the reference model, the weak zone (in the following referred to as 'stepwise weak zone') has an oblique segment in the western Pamir region, connecting Pamir and Hindu Kush. Different geometries of the weak zone (e.g., a straight line) are tested

in other models. The weak zone has opposite dip polarities in the Hindu Kush and in the Pamir region, respectively. The absolute dip angle is however the same (Figs. 2b–2c). We assume that these weak zones with opposite polarities are inherited structures from previous shortening/thrusting events. The lithosphere is uniform in the entire model domain composed of upper crustal (25 km), lower crust (10 km) and mantle lithosphere (85 km). A thin sticky air layer (20 km) and a thick asthenospheric mantle layer (256 km) are imposed on top of and beneath the continental lithosphere, respectively.

A constant temperature boundary condition is employed at the upper and lower boundaries, and a zero heat flux boundary condition is used for the side boundaries. The temperature field is prescribed using a piecewise linear temperature profile with surface, Moho and lithosphere–asthenosphere boundary (LAB) temperatures of 0°C , 500°C and 1300°C (Fig. 2d). The Moho temperature is commonly used as a simplified indicator of the thermal and rheological lithosphere layering, which affects the crustal and lithospheric mantle strength and therefore the lithospheric dynamics (e.g., Geydan et al., 2008; Liao and Gerya, 2017). The moderate Moho temperature of 500°C is used in this study based on our previous test (Liao and Gerya, 2017). Below the LAB, an adiabatic temperature profile with a gradient of $0.5^{\circ}\text{C}/\text{km}$ is prescribed. All boundaries are free slip. An additional internal boundary condition is prescribed to achieve compression of the Indian plate with a constant velocity, e.g., 3 cm/yr in the reference model (e.g., Avouac, 2015).

4. Model results

4.1. Reference model evolution

The evolution of the reference model is shown in temporal snapshots in Fig. 3. The onset time of the model evolution (0 Ma)

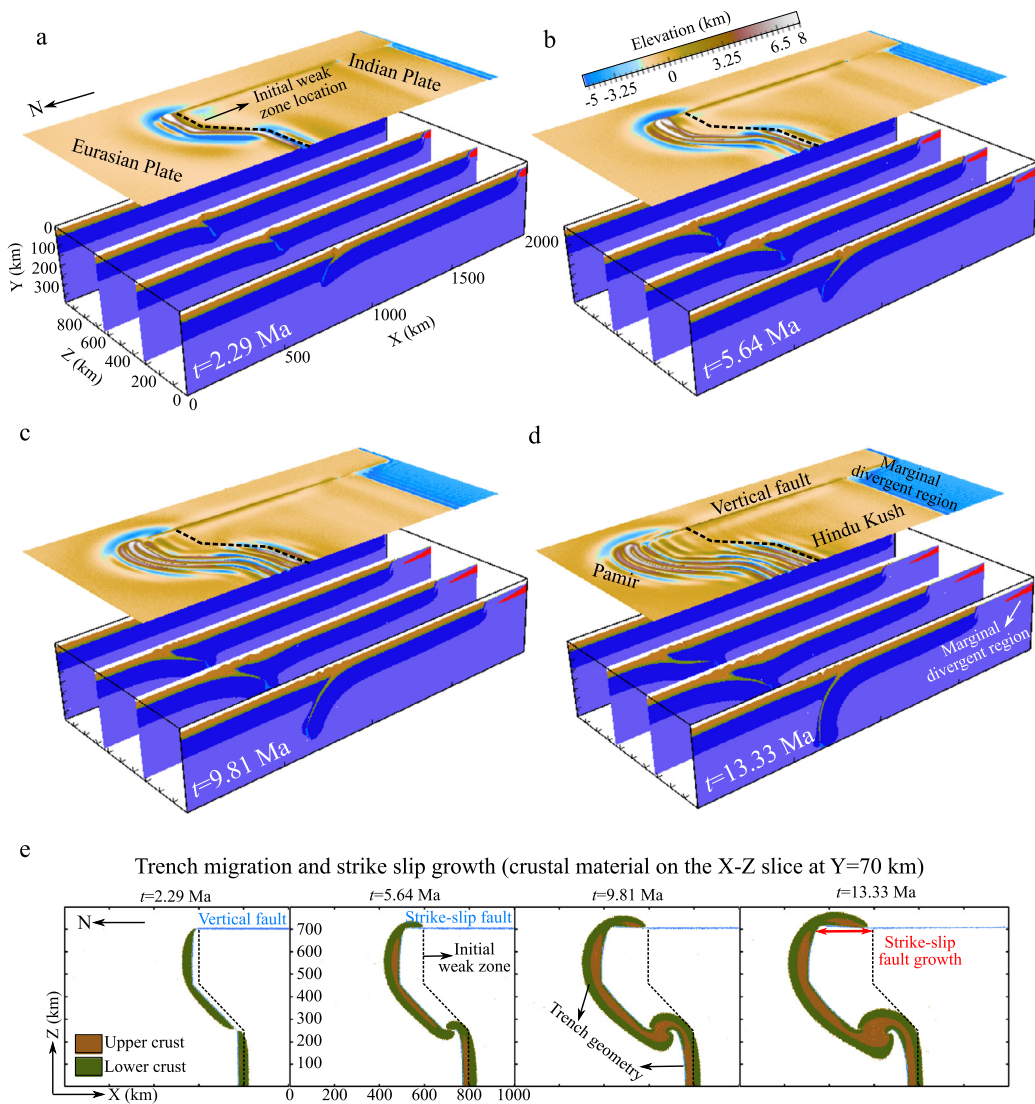


Fig. 3. Evolution of the reference model shown by topography (top) and lithology (bottom). Color coding of lithology as in Fig. 2. (a) Onset of continental collision along the prescribed weak zone. (b) Initiation of continental subduction. (c–d) Enhanced deformation with curved collisional belt on the surface and opposite polarities of the subduction zones. (e) Trench migration and strike-slip fault growth in the Pamir region. Trench geometry is represented approximately by the distribution of crustal material at 70 km depth. (For interpretation of the references to color in this figure, the reader is referred to the web version of this article.)

would correspond to ~ 10 Ma in geological time, since the two opposing continental collision/subduction mainly occurred in the last 10 Ma (e.g., Kufner et al., 2016). As the Indian plate moves towards the Eurasian plate, continental collision occurs and shortening accumulates along the pre-defined weak zone, separating the two lithospheric plates (Fig. 3a). High elevation is formed along the collisional belt. With ongoing convergence, continental subduction initiates (Figs. 3b–3d). The different polarities of the subducting slabs are a result of the predefined opposite dipping polarities of the weak zone. The upper crust is largely shortened and thickened at shallow depths, while the lower crust and mantle lithosphere subduct. A significant orogenic curvature is formed in the Pamir region (Figs. 3d–3e). Although the initial weak zone is stepwise, the curvature of the Pamir region is increasingly smoothed with time (Fig. 3d). Collisional deformation migrates northward as a consequence of the indentation of the Indian plate (Fig. 3d). In the Pamir region, subduction retreats to the north with an increasing offset between the trench and the initial weak zone (Fig. 3e). Meanwhile, the strike-slip fault on the east of the Indian plate propagates to the north (Fig. 3e). Detailed discussion based on the results of the reference model is given in section 5.

4.2. Varied model setups

It is difficult to speculate on the initial geometry of the Indian and Asian margins, prior to the collisional deformation, related to the northward offset of the Pamir. We therefore tested the effect of different initial model configurations (Fig. 4 and Table S3). We focused on the geometry of the marginal vertical fault and the preexisting weak zone as these represent the combined effect of Indian's and Asian's margin in these models (Fig. 4). The influence of the following factors on model evolution is tested (Figs. 4–5), with respect to the effects of (1) the existence of the marginal vertical fault to the east, (2) the lateral (north–south) extend of the marginal vertical fault, (3) the geometry of the weak zone, and (4) the changes in convergence rate.

(1) In the first test model (Fig. 4a), the marginal vertical fault to the east (right) of the Indian plate is removed. The predominant feature is that collision and subduction extend to the rear part along the strike of the weak zone, since the entire Indian plate indents northward. Besides, plate underthrusting (resulted in plate thickening) rather than subduction occurs in the rear part of the model (Fig. 4a), since the weak zone does not extend to the end of

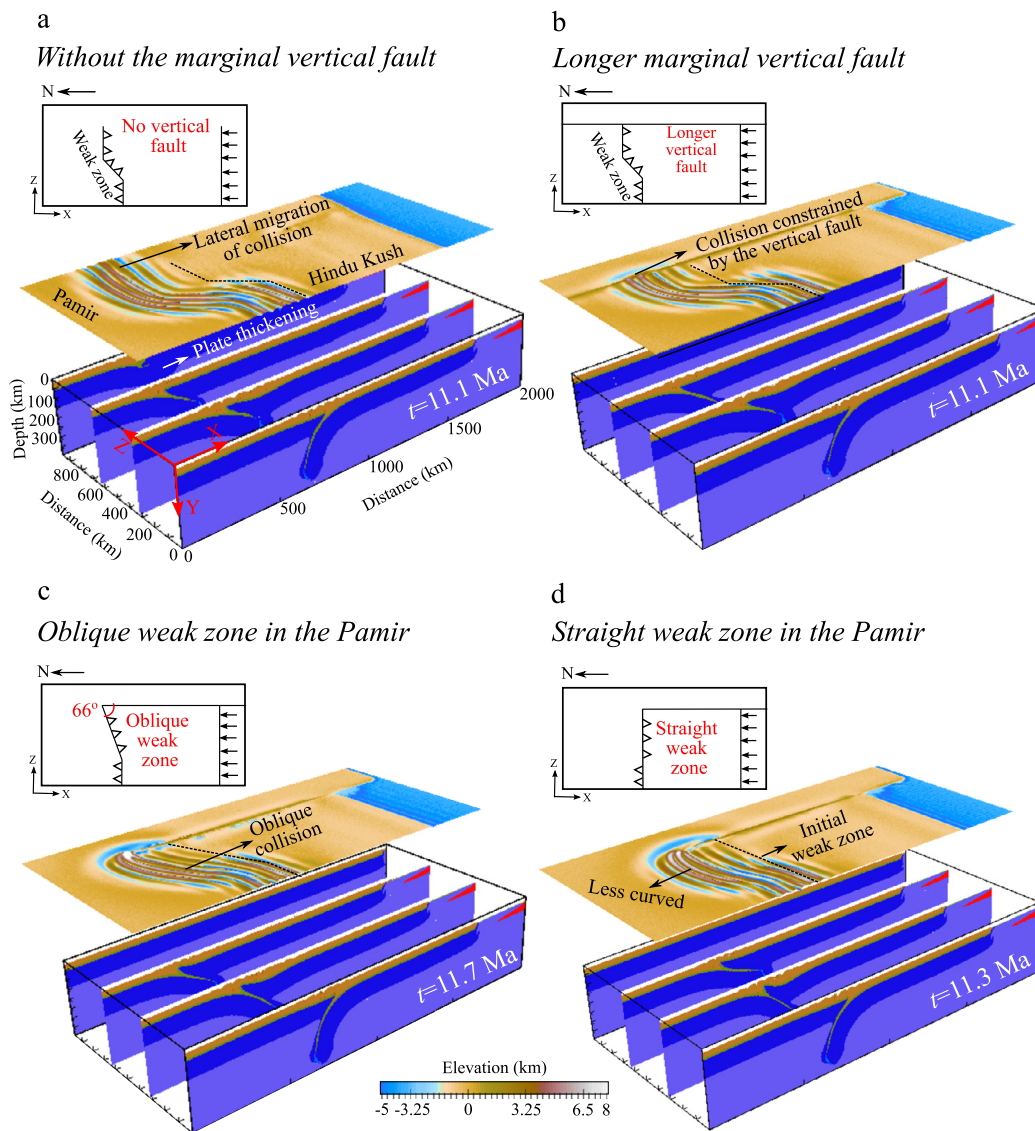


Fig. 4. Model tests of varied setups based on the reference model. Model test with (a) no vertical fault; (b) the longer marginal vertical fault; (c) an oblique and (d) a straight weak zone in the Pamir. Sketches show model setups on map view, with modifications emphasized in red. (For interpretation of the references to color in this figure legend, the reader is referred to the web version of this article.)

the model domain. (2) In the second model (Fig. 4b), the marginal vertical fault to the east (right) of the Indian plate is longer. The curvature of the collisional belt in the eastern end of the Pamir region is reduced and lateral migration of collisional deformation is largely constrained by the preexisting marginal vertical fault. (3) In the third and fourth cases (Figs. 4c and d), the influence of the geometry of the weak zone is tested. The third model has a straight oblique weak zone prescribed in the Pamir region (Fig. 4c). Although curved collisional belts are formed in the transition zone between Hindu Kush and Pamir, the arcuate geometry of the Pamir orogen is less significant. With a straight orthogonal weak zone prescribed in the fourth model (Fig. 4d), much less curved Pamir orogen is established.

(4) The influence of the convergence rate is tested based on the reference model (Fig. 5 and Table S3). Although the Indian plate moves northward with respect to the stable Eurasian plate at high velocities $\sim 3\text{--}4$ cm/yr (Aouac, 2015), the convergence is distributed in the Pamir region (from the southern edge of the Himalaya to the Tian Shan), and roughly half of the convergence might be absorbed along the northern margin of the Pamir region (Burtman and Molnar, 1993). We therefore test models using convergence velocities from extremely slow (2 cm/yr) to extremely

fast (5 cm/yr). Model results suggest an increase in convergence rate leads to a slight increase in the curvature of the collisional belts (Figs. 5a and b). Besides, high convergence velocities largely promote collisional deformation and surface expression (Fig. 5a). The computed mean surface uplift (averaging the positive surface elevation) increases with the increase of convergence velocity (Fig. 5c). This is consistent with natural observations that show relatively low surface elevation in the Alps and high elevation in the Himalaya–Tibet and Andes, controlled by slow and high convergence rates, respectively (e.g., Pusok and Kaus, 2015). Higher boundary velocities correlate with higher boundary force (e.g., Liao and Gerya, 2014, 2017), which can thus support higher surface elevation.

5. Discussion

5.1. Geometry of and deformation within the orogens

The Cenozoic Hindu Kush–Pamir orogenic system has an arcuate shape in map view, especially the highly curved Pamir orogen (Burtman and Molnar, 1993; Negredo et al., 2007; Sobel et al., 2013). All models conducted in this study produce curved

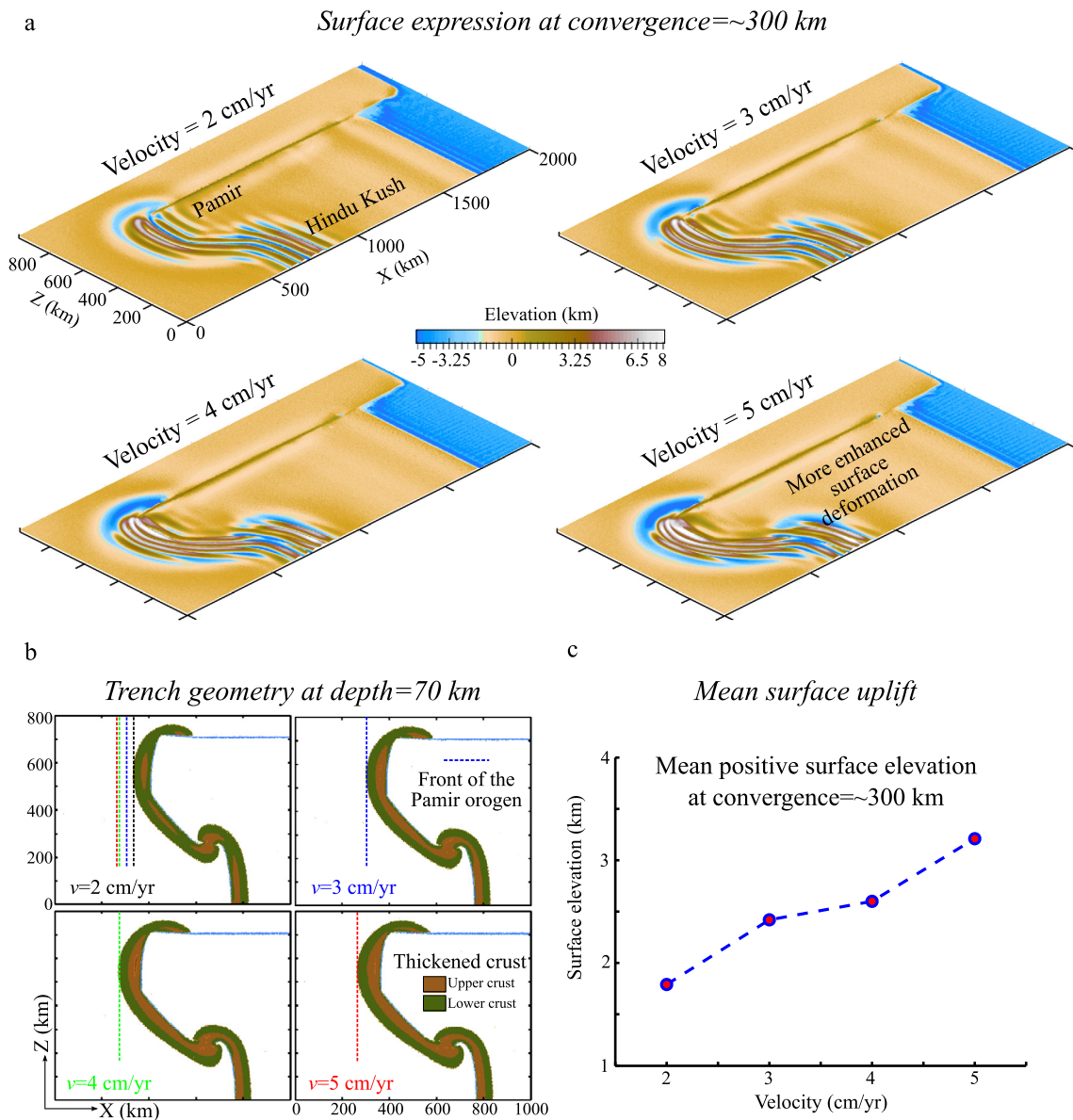


Fig. 5. Effect of convergence velocity on model evolution. The same convergence (~ 300 km) is achieved in all the four models. (a) Model results with varied convergence velocities from 2 to 5 cm/yr. (b) Trench geometry shown by thickened crust at depth of 70 km. Dashed color lines indicate the front of the Pamir orogen. (c) Mean surface uplift influenced by convergence velocities. The mean surface uplift is calculated by averaging the positive surface elevation. (For interpretation of the references to color in this figure legend, the reader is referred to the web version of this article.)

orogens and subduction zones in the Pamir region (Figs. 3–5). However, models with either an oblique straight weak zone or a compression-orthogonal straight weak zone produce clearly less curvature in the Pamir collision/subduction zone than observed in nature. Models with a stepwise weak zone generate pronounced curvatures in the Pamir region, especially at its western margin as this margin is most severely influenced by the oblique segment of the weak zone (Fig. 6a). The presence of this oblique segment in the plate boundary promotes oblique collision and strike-slip, which is consistent with the left-slip transpressional strike-slip faults (e.g., Darvaz and Kapisa–Nuristan faults) observed at the Pamir’s western margin (Fig. 6b). At the Pamir’s eastern margin, our model also creates a slightly curved collision/subduction zone, due to the prescribed marginal vertical fault. Further, the existence of the marginal vertical fault (which evolves to a strike-slip fault) at the Pamir’s eastern margin allows subduction to retreat to the north (Fig. 6a), causing an increasing offset between the trench and the initial weak zone (Fig. 3e) in consistent with observations (Sobel et al., 2013). The strike-slip fault is also considered

as a Subduction–Transform Edge Propagator, or STEP fault, along which slab tearing occurs (Sobel et al., 2013). Vertical slab tearing at the eastern edge of the Pamir orogen is also observed in our model, associating with the northward growth of the strike-slip fault (Fig. 3e). Thus, the deformation pattern of the Pamir region modeled here with an oblique weak zone to the west and a vertical fault to the east yields a situation, consistent with the proposed kinematic models for this region: northwest-directed radial thrusting on the western margin and transpressional right-slip faulting on the eastern margin (Cowgill, 2010). In our model, the western margin of the Hindu Kush is freely sliding due to the free slip boundary condition, representing the presence of the marginal strike-slip fault, i.e., the Chaman fault to the west of the Hindu Kush (Fig. 6a). The free slip boundary prevents the westward propagation of the Hindu Kush orogen. In the eastern part of the Hindu Kush (the transition from Hindu Kush to Pamir), the collision/subduction zone in our model bends slightly northward, which may be connected with the Pamir orogen through transpressional left-slip faulting (e.g., the KN fault). Thus, the overall geometry of

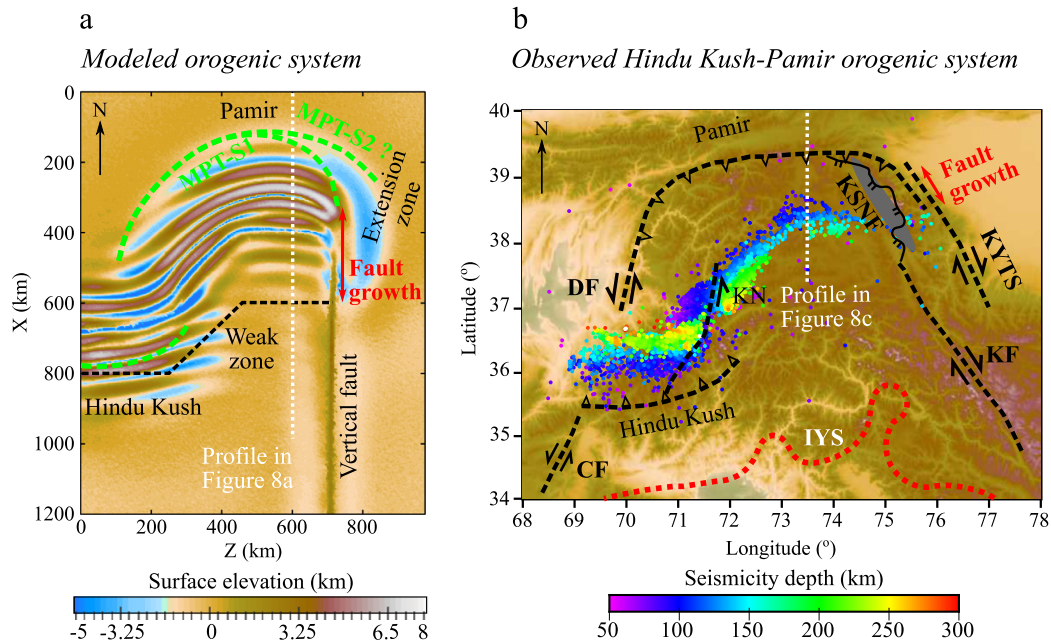


Fig. 6. Comparison of modeled and observed collision/subduction zones. (a) Model results of the curved Hindu Kush–Pamir orogenic system. Green dashed lines indicate the subduction zones. MPT-S1: Main Pamir Thrust of scenario 1. (b) Approximate outline of subduction zones in nature and surface projection of deep (>50 km) seismic events (Kufner et al., 2016). CF: Chaman fault, DF: Darvaz fault, KN: Kapisa–Nuristan fault, IYS: Indus–Yarlung suture, KSNF: Kongur Shan normal fault (extension system), KF: Karakorum fault, KYTS: Kashgar Yecheng transfer system. (For interpretation of the references to color in this figure legend, the reader is referred to the web version of this article.)

the curved Hindu Kush–Pamir orogenic system reproduced in our models is highly similar to observations.

Besides the similar overall geometry reproduced in the Hindu Kush–Pamir orogenic system, our model also resolves the secondary tectonic feature of the region: i.e., an extensional basin at the location of the active north–northwest striking Kongur Shan extension system in the northeastern Pamir (Fig. 6b, Robinson et al., 2004, 2007). The depression area in our model, which can be interpreted as an extension zone, is developed due to the lateral extend of the Pamir subduction (Fig. 6a; see also different perspectives of the depression in Fig. S1), and can be compared with the Kongur Shan extension system. However, due to our simplified model geometry we can hardly discriminate which of the two major strike-slip systems (the Karakorum fault and the Kashgar–Yecheng transfer system) to the Pamir’s east represents the strike-slip fault in our model. The Kashgar–Yecheng transfer system (KYTS) connects to the northern Pamir, while the Karakorum fault (KF) transfers dextral slip into the South and Central Pamir, where it is distributed in different splay systems (e.g., Cowgill, 2010; Schurr et al., 2014). The KF terminates to the south of the active Kongur Shan extension system. Thus, not necessarily the KF but the KYTS must have accommodated a large amount of the northward offset of the Pamir. If the prescribed vertical fault in our model would correspond to the KYTS (Fig. 6a), the extension zone reproduced in the model is located to the east of the strike-slip fault, which is inconsistent with observations (Fig. 6b). Alternatively, we can interpret the prescribed vertical fault in the model as the KF. In this case, the locations of the extension zone and the strike-slip fault are more consistent with observations. However, the Pamir slab was postulated to have retreated along the KYTS in the northern Pamir (Cowgill, 2010; Sobel et al., 2013). We test two parallel vertical faults (one represents the KYTS and the other represents the KF) which does not show significant changes from the reference model (Fig. S2). Given the simple model in this study, it is difficult to resolve what the sequence of events on these faults was.

5.2. Varying subduction depth and slab steepness

One of the striking features of the Hindu Kush–Pamir orogenic system is their differences in subduction depth and slab steepness (Figs. 1 and 7). The continental slab underneath the Hindu Kush is steeper ($\sim 80^\circ$) and deeper (>500 km) than the one beneath the Pamir region ($\sim 45^\circ$ and >300 km, Negredo et al., 2007; Sippl et al., 2013; Kufner et al., 2016). Our models reproduce these varied slab depth and steepness (Figs. 7a and b). Although the initial dip angles of the weak zone in the Hindu Kush and Pamir are identical (with opposite polarities, Fig. 2c), a steeper and deeper subduction zone is formed in the Hindu Kush. The formation of different dip angles and subduction depths in the opposing subduction zones can be explained by the one-sided indentation of the Indian plate (Figs. 7c and d). In the Pamir region, the upper plate drives subduction and the lower plate is bending and retreating in response to the advancing upper plate. In the Hindu Kush region, the lower plate drives subduction and advances towards the upper plate (Fig. 7d). As a response to the fast indentation rate, the shallow part of the down-going slab advances faster than the deeper part, and the subducted slab becomes steeper. A faster convergence rate promotes the formation of a deeper and steeper subducted slab underneath the Hindu Kush (Fig. S3). Thus, with sufficient convergence, the subducted slab underneath the Hindu Kush may even bend over (Figs. 1b and 4).

5.3. Continental subducted versus escape flow

We further compare the structure of the subducted lithosphere in our model (Figs. 8a and b) with geophysical observations along a north–south cross section through the Pamir orogen (Fig. 8c): the receiver function profile shows thickened crust and subducted lower crust (Schneider et al., 2013). Our model presents comparable results: the upper crust is largely shortened/thickened at shallow depths, while the lower crust is subducted with the mantle lithosphere (Figs. 8a and b). Subduction of only the lower crust is promoted by the weakly coupled upper and lower crust (Fig. 8b).

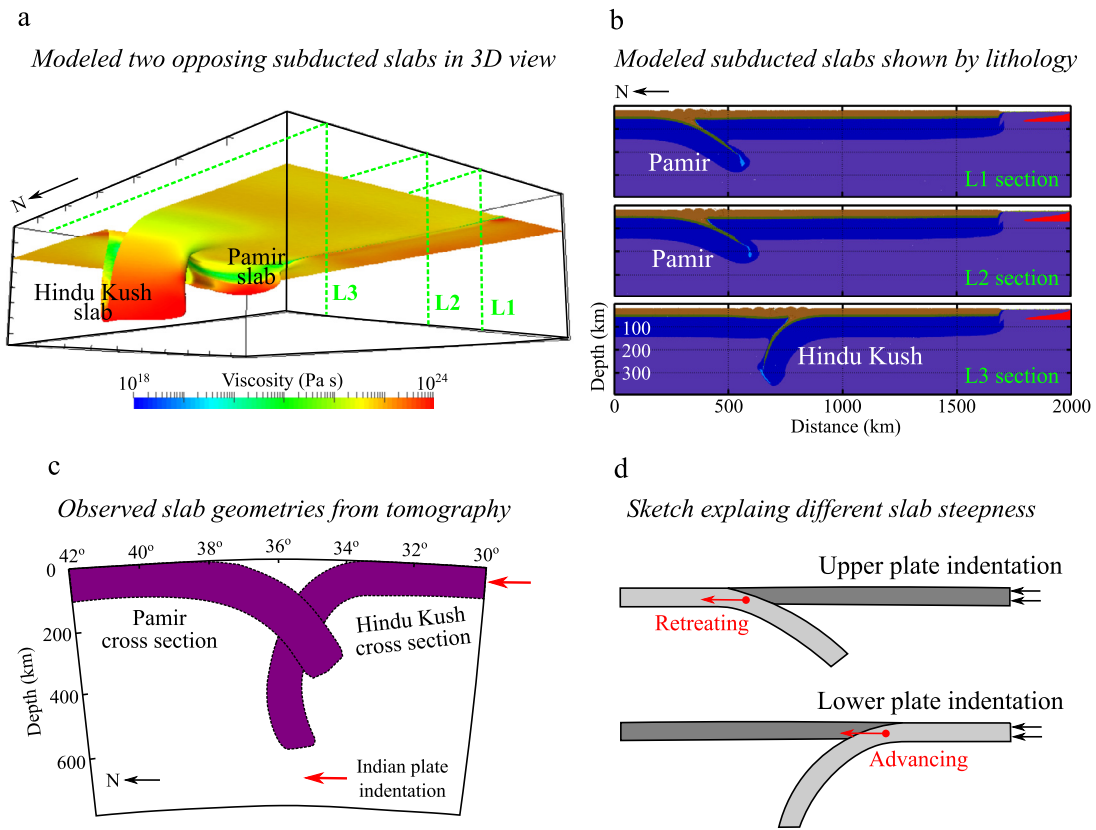


Fig. 7. Modeled and observed geometries of the two opposing subducted slabs. (a) Modeled subducted slabs shown in 3D view. Color indicates viscosity. (b) Slab geometry shown by lithology. Locations of the cross sections are labeled in (a). (c) Observed slab geometries in the Hindu Kush and Pamir orogens. The slab outlines are drawn based on the tomography sections shown in [Negredo et al. \(2007\)](#) and [Kufner et al. \(2016\)](#). (d) Sketch explaining the varied subduction depth and slab steepness: upper plated indentation versus lower plate indentation. (For interpretation of the references to color in this figure legend, the reader is referred to the web version of this article.)

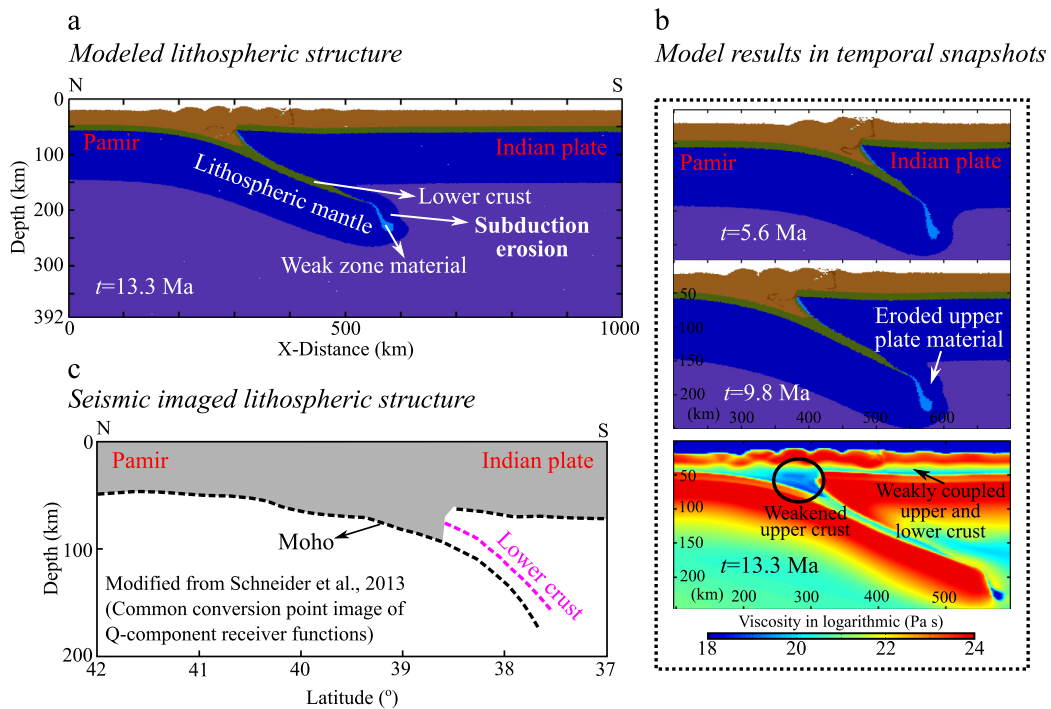


Fig. 8. Structure of the subducted lithosphere. (a) Model results along a north–south profile in the Pamir region showing subducted lower crust and subduction erosion. (b) Temporal evolution shown in lithology and viscosity. (c) A north–south seismic cross section in the Pamir region modified from [Schneider et al. \(2013\)](#). Locations of the cross sections are shown in [Fig. 6](#).

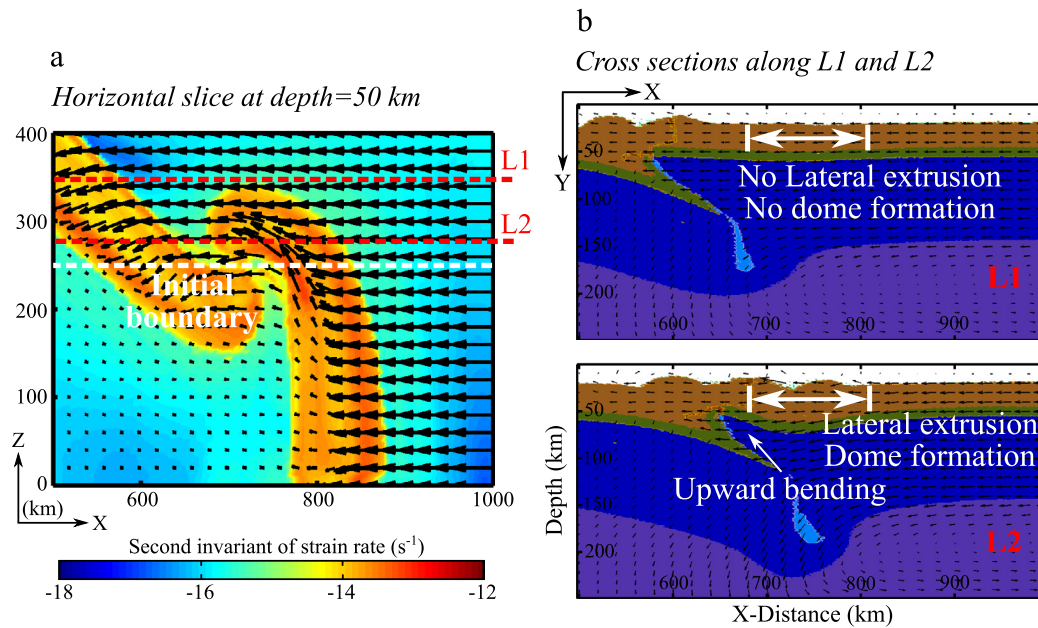


Fig. 9. Lateral crustal flow along collisional belts based on the reference model. (a) A horizontal slice at 50 km depth showing lateral crustal flow. The lower part of the thickened upper crust becomes weak, promoting lateral crustal flow along the trench. Arrows are velocity vectors of V_x and V_z . (b) Cross sections along the L1 and L2 profiles showing lithospheric deformation. Dome formation and upward bending of the proximal upper plate due to lateral crustal extrusion are shown. Arrows are velocity vectors of V_x and V_y .

Liao and Gerya (e.g., 2017), for instance, showed that the subduction of the entire crust is only possible if upper and lower crust were fully coupled. As this is clearly not the case in the Pamir, our models help to constrain the amount of coupling between the different crustal units in this region. Additionally to the decoupling between the two crustal layers, our model shows subduction erosion (Figs. 4, 5 and 8; the downgoing plate scrapes material from the overriding plate). Subduction erosion was proposed to occur along the Main Pamir Thrust as it accommodates large amounts of shortening without significant upper-plate exhumation in the middle Miocene (Sobel et al., 2013). Subduction erosion in our models is created as the continental plates have a relatively strong subduction interface without the lubrication from slab dehydration, which occurs in oceanic subduction zones.

In our numerical experiments, we observe strong crustal flow along the main collisional belts (Fig. 9). Unlike the large scale lower crustal flow proposed in the eastern Tibetan Plateau (e.g., Clark and Royden, 2000), the small scale crustal flow only occurs along and flows parallel to the main collisional belts. The laterally flowing crustal material consists mainly of the thickened upper crust, which does not subduct but largely deforms/shortens at shallow depths. The deeper part (~ 30 km deeper from the crustal surface) of the thickened upper crust weakens and becomes ductile (e.g., Fig. 8b), and thus flows laterally along the main collisional belts in response to the continuous convergence (Fig. 9a). As a consequence to the lateral extrusion of the ductile crust, the adjacent crustal layer becomes thicker forming crustal domes and the proximal upper plate bends slightly upwards (Fig. 9b). This type of bending is observed for example in the Western Alps and has been discussed in previous studies (e.g., Faccenda et al., 2008). Although upward plate bending is not addressed in the Hindu Kush–Pamir orogenic system, lateral flow of the weakened ductile crust is possible and may facilitate dome formation. Robinson et al. (2007) proposed that the formation of the Central Pamir gneiss domes is due to the upward extrusion of the thickened middle and lower crust during north–south convergence. East–west orogen-parallel crustal flow in the Pamir was discussed in previous studies (Stübner et al., 2013; Rutte et al., 2017). Based on geological observations (e.g., along-strike flow lineation in recumbent

folds, orogen-parallel extension and dextral wrenching in fold-and-thrust belts), they emphasized the large scale lateral extrusion of ductile crust occurred in the Pamir during north–south shortening (e.g., Rutte et al., 2017). Although the lateral crustal flow occurs locally in our models (along the main collisional belts), it may give a broad implication for the dome formation in the Pamir region and the proposed westward extrusion of the western Pamir (Schurr et al., 2014): weakened ductile crust flows laterally from more intensively compressed areas to relatively less compressed regions.

5.4. Intermediate-depth earthquakes

The Hindu Kush–Pamir orogenic system is characterized by clusters of intermediate (50–300 km) depth earthquakes, with their majority occurring at 100 and 200 km depth (Fig. 10a, e.g., Sippl et al., 2013; Kufner et al., 2016). Their origin is enigmatic. Dehydration embrittlement is frequently invoked to explain intermediate-depth earthquakes in oceanic subduction zones (Kirby et al., 1996; Hacker et al., 2003), where water is released from hydrated oceanic slabs. Unlike oceanic subducted slabs, continental subducted slabs do not experience significant slab hydration in the early subduction stage. Therefore, slab dehydration and dehydration embrittlement is not likely occurring in the Hindu Kush and Pamir continental subduction zones. Thus, thermal runaway is a more likely mechanism than dehydration embrittlement to generate intermediate-depth earthquakes in this region. Thermal runaway describes the feedback between shear heating induced weakening and temperature-dependent rock rheology. Once heat production in a shear zone exceeds heat diffusion, the rock is continuously weakened. This results in an increase in strain rate, which in turn increases the amount of heat production. This positive feedback loop eventually results in a catastrophic process where temperatures might even reach the liquidus (Hobbs et al., 1986). High stresses are needed for this mechanism to be effective, but it has been shown that grain size reduction significantly reduces the critical stress required for thermal runaway (Thielmann et al., 2015). Along the subduction interface, shear heating can be very intense (e.g., Thielmann and Kaus, 2012).

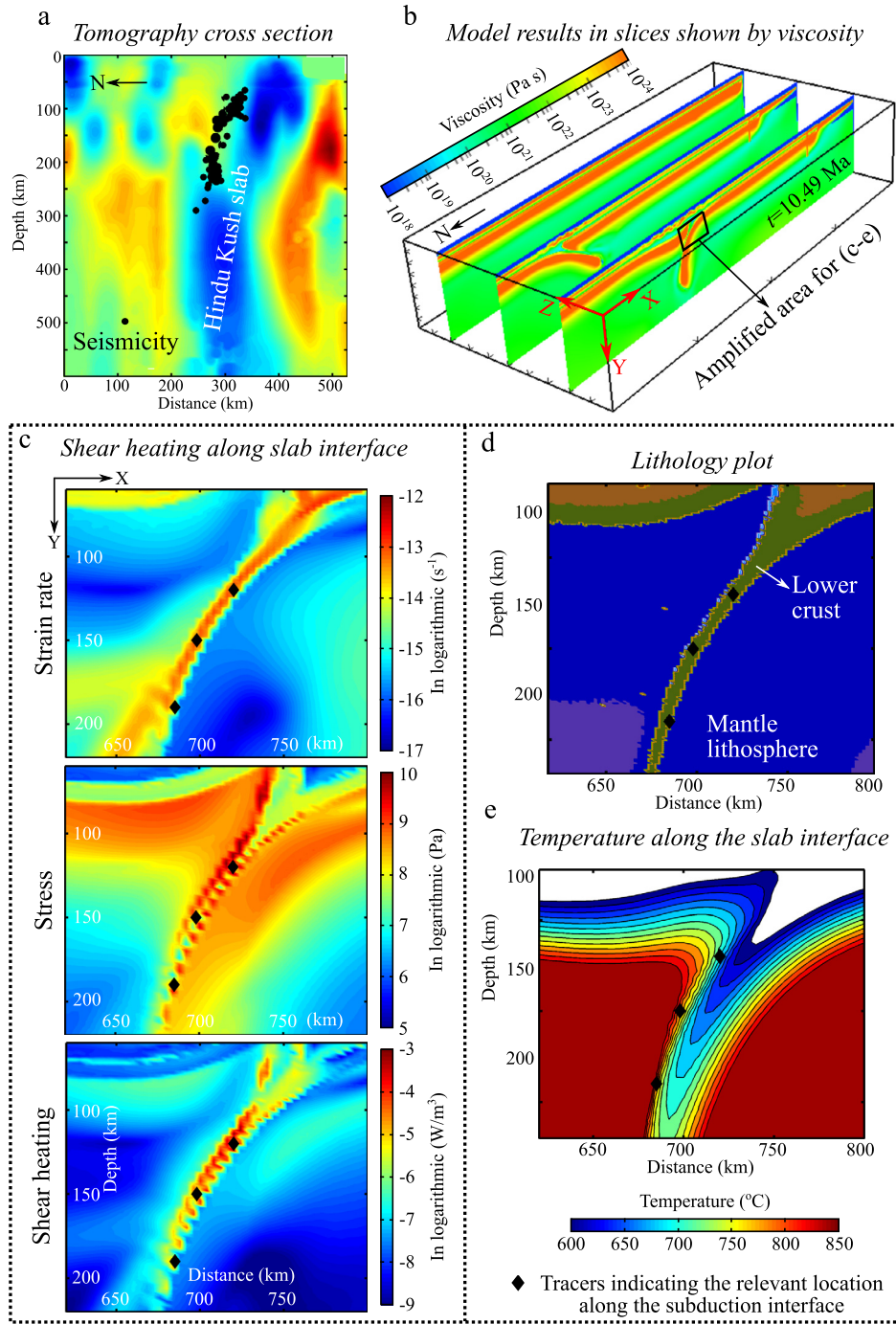


Fig. 10. Possible conditions for thermal runaway/shear instability causing intermediate-depth earthquakes. (a) Seismicity on a tomography cross section. See the profile location AA' in Fig. 1. (b) Model results at $t = 10.49$ Ma. The black rectangle marks the amplified area shown in the subsequent plots. (c) Second invariants of strain rate and stress, and the resulted shear heating. (d) Lithology distribution showing the distribution of the lower crust along the subduction interface. (e) Temperature distribution along subduction interface. Temperature falls in the reasonable range for intermediate-depth earthquakes (600–850 °C, e.g., Kelemen and Hirth, 2007, and references therein).

In order to investigate if thermal runaway could potentially occur and lead to intermediate-depth seismicity in our model, we chose one representative cross section along the Hindu Kush orogen (Fig. 10). Choosing an example cross section along the Pamir would yield similar results (significant shear heating along subduction interface perturbed by the lower crust; see discussion below). The along-strike variation in shear heating is not investigated in this study. The model results presented here yield strong shear heating along the subduction interface, which is a result of large stresses (due to low temperatures at the subduction interface) and strain rates (Fig. 10c). The presence of the lower crust

(and thus a different material, Fig. 10d) represents a strong rheological perturbation (in this case lower crustal material is less viscous than mantle material), which additionally favors thermal runaway (e.g., John et al., 2009). The combination of low temperatures and large stresses thus favors the occurrence of grain size assisted thermal runaway. Intermediate-depth earthquakes occur mainly between 600 and 850 °C (Kelemen and Hirth, 2007, and references therein). Our models show consistent results with the temperature along the subduction interfaces falling in the range of 600–850 °C (Fig. 10e).

5.5. Comparison with the Alpine orogen

Our above presented models are not only aimed to understand the evolution of the 3D geometry within the Hindu Kush–Pamir subduction system, but are also designed to understand more general characteristics of complex opposing continental subduction systems in general. We compare some of the predominant features reproduced in our models to the Alpine orogen in the Europe (Fig. S4). First, the formation of the remarkable arcuate geometry of the Pamir orogen can be compared to that of the Western Alpine arc. In our models, the formation of the curved Pamir orogen is promoted largely by the presence of the oblique segment of the stepwise weak zone, since collisional deformation accumulated in front of the oblique weak zone. This could also be the case for the development of the Western Alpine arc. The strike of the Western and Central Alpine orogen is not straight during the collision between the European and Adriatic plate since ~ 35 Ma; the Western Alps trends NE–SW and the Central Alps trends W–E (Fig. S4a), which shares similarity with the weak zone in the Pamir orogen. The northward indentation with counterclockwise rotation of the Adriatic plate has been regarded as the main driving mechanism for the establishment of the Western Alpine arc (e.g., [Schmid and Kissling, 2000](#)), which is analogous to the dynamic evolution of the Pamir orogen shown in our models. Second, a recent high-resolution P-wave tomography data reveals the varied depth and steepness of the two opposing subducted slabs in the Alps and Dinarides (Fig. S4b, [Zhao et al., 2016](#)). Similar to the Indian plate acting as the downgoing plate in the Hindu Kush and the overriding plate in the Pamir, the northward indenting Adriatic plate behaves as the downgoing plate in the Dinarides and the overriding plate in the Alps. The subducted Adriatic plate underneath the Dinarides is slightly deeper and steeper than the subducted European plate beneath the Alps (Fig. S4b). This feature could also be explained by the one-sided indentation of the Adriatic plate (Figs. 7d and S4).

5.6. Model restrictions

Our model geometry is deliberately kept simple. We wanted to understand the complex 3D geometry of the Hindu Kush–Pamir orogenic system as a case example (Sections 5.1 and 5.2), but also aimed to address more general questions related to continental subduction (Sections 5.3 and 5.4). Therefore we did not want to mask the effects of changing model parameters by a too complex initial model setting or too many free parameters.

Different tectonic features, specific for the Pamir–Hindu Kush region, might need further investigation which are not explored in this study (which is tailored to investigate the time span between subduction initiation and termination). Apart from the initiation scenario chosen here (two opposite dipping weak zones, inherited from former tectonic events), other scenarios might be possible (e.g., short remnant subducted slab beneath the Hindu Kush, over thickening of Asian lithosphere beneath the Pamir prior to subduction initiation; [Tympele, 2015](#)). Another striking feature, characteristic for the Hindu Kush, is the on-going break-off of the subducting Indian slab ([Kufner et al., 2017](#)). This break-off might be initiated as the lithosphere subducted beneath the Hindu Kush is not purely continental, but rather Indian's stretched margin ([Kufner et al., 2016](#)). We experimented with thinner lithosphere beneath the Hindu Kush (Fig. S5), which yielded a steeper slab than the reference model. However, modeling the final pinching of the Hindu Kush slab is not the scope of this paper, as a larger vertical model domain would be required. Finally, the topography formed in our models is partly dissimilar to the smooth topography observed in nature. This is due to the simplified surface process that we use. The prescribed high sedimentation/erosion levels in our models

(i.e., 10 km below/above the initial crustal surface, respectively) do not produce significant sedimentation/erosion on the surface, resulting in high uplifts and deep depressions. The model with lower sedimentation/erosion levels (i.e., 5 km below/above the initial crustal surface, respectively) produces much more significant surface erosion/sedimentation, forming relatively smooth surface expression (Fig. S6). Besides, different model parameters, such as the thickness of the lower crust (Fig. S5), may also influence the surface expression.

6. Conclusion

In this study, we use a 3D geodynamic model to investigate the dynamic evolution of the complex Hindu Kush–Pamir collision/subduction system and to understand the dynamics of continental subduction in general. A set of 3D numerical models are conducted with varied model setups. Our model results shed lights on the dynamic evolution of the two opposing continental subduction zones. The following conclusions can be drawn based on our model results.

(1) Two opposite dipping collision/subduction zones are developed in the Hindu Kush–Pamir region as a consequence to the prescribed opposite dipping weak zones existed in the lithosphere prior to the onset of subduction. After subduction initiation, the Hindu Kush subducted slab naturally develops a much deeper penetrating and steeper dipping geometry than the Pamir subducted slab. This geometric difference is created as the dip-direction of the Pamir slab and Indian plate convergence oppose each other, whereas they match in the Hindu Kush.

(2) The arcuate but asymmetric geometry of the Pamir orogen is promoted by an initially oblique segment in the weak zone in the western Pamir, i.e., the asymmetric geometry of the Indian indenter, and a major strike-slip fault at the eastern Pamir margin.

(3) Continental subduction occurs promoted by weakly coupled upper and lower crust: the upper crust is largely deformed/shortened at shallow depths, whereas the lower crust subducts attached to the mantle lithosphere. The lateral extrusion of weakened ductile crust may facilitate dome formation locally.

(4) Significant shear heating is generated along the subduction interface that consists of the lower crust. This may provide a potential condition for thermal runaway that could cause intermediate-depth earthquakes.

(5) Additionally, several secondary tectonic features observed in nature are reproduced in our models. A marginal strike-slip fault migrates northward during the Pamir indentation and a north-northwest striking extension zone is formed in the northeast of the Pamir region due to the radial thrusting.

(6) Finally, model results are compared to the Alpine orogen. The formation of the Western Alpine arc and the variation (depth and steepness) of the two opposing subducted slabs underneath the Alps and the Dinarides are similar and comparable to the Hindu Kush–Pamir orogenic system.

Acknowledgements

This research is supported by Swiss-AlpArray SINERGIA project CRSII2_154434/1 by Swiss National Science Foundation (SNSF). J.L. appreciates the discussion with Daniel Rutte. M.T. was supported by the Bayerisches Geoinstitut Visitor's Program. S.-K.K. thanks the support from the TIPTIMON project (support code 03G0809). We note that there are no data sharing issues since all of the numerical information is provided in the figures produced by solving the equations in the paper. Users can access data from this paper by contacting the authors.

Appendix A. Supplementary material

Supplementary material related to this article can be found online at <https://doi.org/10.1016/j.epsl.2017.10.005>.

References

- Avouac, A.P., 2015. Mountain building: from earthquakes to geologic deformation. In: Schubert, G. (Ed.), *Treatise on Geophysics*, second edition, pp. 381–432.
- Beaumont, C., Jamieson, R.A., Nguyen, M., Lee, B., 2001. Himalayan tectonics explained by extrusion of a low-viscosity crustal channel coupled to focused surface denudation. *Nature* 414, 738–742.
- Burg, J.P., Gerya, T., 2005. The role of viscous heating in Barrovian metamorphism of collisional orogens: thermomechanical models and application to the Lepontine Dome in the Central Alps. *J. Metamorph. Geol.* 23, 75–95. <http://dx.doi.org/10.1111/j.1525-1314.2005.00563.x>.
- Burtman, V.S., Molnar, P., 1993. Geological and geophysical evidence for deep subduction of continental crust beneath the Pamir. *Spec. Pap., Geol. Soc. Am.* 281, 1–76. <http://dx.doi.org/10.1130/SPE281-p1>.
- Capitanio, F.A., 2014. The dynamics of extrusion tectonics: insights from numerical modeling. *Tectonics* 33, 2361–2381. <http://dx.doi.org/10.1002/2014TC003688>.
- Chen, L., Gerya, T.V., 2016. The role of lateral lithospheric strength heterogeneities in orogenic plateau growth: insights from 3-d thermo-mechanical modeling. *J. Geophys. Res.* 121, 3118–3138. <http://dx.doi.org/10.1002/2016JB012872>.
- Clark, M.K., Royden, L.H., 2000. Topographic ooze: building the eastern margin of Tibet by lower crustal flow. *Geology* 28, 703–706.
- Cowgill, E., 2010. Cenozoic right-slip faulting along the eastern margin of the Pamir salient, northwestern China. *Geol. Soc. Am. Bull.* 122, 145–161. <http://dx.doi.org/10.1130/B265201>.
- Faccenda, M., Gerya, T.V., Chakraborty, S., 2008. Styles of post-subduction collisional orogeny: influence of convergence velocity, crustal rheology and radiogenic heat production. *Lithos* 103, 257–287. <http://dx.doi.org/10.1016/j.lithos.2007.09.009>.
- Gerya, T.V., 2013. Three-dimensional thermomechanical modeling of oceanic spreading initiation and evolution. *Phys. Earth Planet. Inter.* 214, 35–52. <http://dx.doi.org/10.1016/j.pepi.2012.10.007>.
- Gueydan, F., Morency, C., Brun, J.P., 2008. Continental rifting as a function of lithosphere mantle strength. *Tectonophysics* 460, 83–93. <http://dx.doi.org/10.1016/j.tecto.2008.08.012>.
- Hacker, B.R., Peacock, S.M., Abers, G.A., Holloway, S.D., 2003. Subduction factory 2. Are intermediate-depth earthquakes in subducting slabs linked to metamorphic dehydration reactions? *J. Geophys. Res.* 108. <http://dx.doi.org/10.1029/2001JB001129>.
- Hobbs, B., Ord, A., Teyssier, C., 1986. Earthquakes in the ductile regime? *Pure Appl. Geophys.* 124, 309–336.
- John, T., Medvedev, S., Rüpke, L.H., Andersen, T.B., Podladchikov, Y.Y., Austrheim, H., 2009. Generation of intermediate-depth earthquakes by self-localizing thermal runaway. *Nat. Geosci.* 2, 137–140. <http://dx.doi.org/10.1038/NNGEO419>.
- Kelemen, P.B., Hirth, G., 2007. A periodic shear-heating mechanism for intermediate-depth earthquakes in the mantle. *Nature* 446, 787–790. <http://dx.doi.org/10.1038/nature05717>.
- Király, Á., Capitanio, F.A., Funicello, F., Faccenna, C., 2016. Subduction zone interaction: controls on arcuate belts. *Geology* 44, 715–718.
- Kirby, S., Engdahl, R.E., Denlinger, R., 1996. Intermediate-depth intraslab earthquakes and arc volcanism as physical expressions of crustal and uppermost mantle metamorphism in subducting slabs. In: *Subduction Top to Bottom*, vol. 96, pp. 195–214. <https://doi.org/10.1029/GM096p0195>.
- Kufner, S.K., Schurr, B., Haberland, C., Zhang, Y., Saul, J., Ischuk, A., Oimahmadov, I., 2017. Zooming into the Hindu Kush slab break-off: a rare glimpse on the terminal stage of subduction. *Earth Planet. Sci. Lett.* 461, 127–140. <http://dx.doi.org/10.1016/j.epsl.2016.12.043>.
- Kufner, S.K., 2016. *Lithospheric Structure and Seismotectonic Setting of the Hindu Kush, the Tajik-Afghan Basin and the Western Pamir from Analysis of Local- and Teleseismic Data*. Ph.D. thesis. Freie Universität, Berlin.
- Kufner, S.K., Schurr, B., Sippl, C., Yuan, X., Ratschbacher, L., Ischuk, A., Murodkulov, S., Schneider, F., Mechie, J., Tilmann, F., 2016. Deep India meets deep Asia: lithospheric indentation, delamination and break-off under Pamir and Hindu Kush (Central Asia). *Earth Planet. Sci. Lett.* 435, 171–184. <http://dx.doi.org/10.1016/j.epsl.2015.11.046>.
- Li, Z.H., Xu, Z.Q., Gerya, T.V., 2011. Flat versus steep subduction: contrasting modes for the formation and exhumation of high- to ultrahigh-pressure rocks in continental collision zones. *Earth Planet. Sci. Lett.* 301, 65–77. <http://dx.doi.org/10.1016/j.epsl.2010.10.014>.
- Li, Z.H., Xu, Z., Gerya, T., Burg, J.P., 2013. Collision of continental corner from 3-d numerical modeling. *Earth Planet. Sci. Lett.* 380, 98–111. <http://dx.doi.org/10.1016/j.epsl.2013.08.034>.
- Liao, J., Gerya, T., 2014. Influence of lithospheric mantle stratification on craton extension: insight from two-dimensional thermo-mechanical modeling. *Tectonophysics* 531, 50–64. <http://dx.doi.org/10.1016/j.tecto.2014.01.020>.
- Liao, J., Gerya, T., 2017. Partitioning of crustal shortening during continental collision: 2-d thermomechanical modeling. *J. Geophys. Res.* 122, 592–606. <http://dx.doi.org/10.1002/2016JB013398>.
- Menant, A., Sternai, P., Jolivet, L., Guillou-Frottier, L., Gerya, T., 2016. 3D numerical modeling of mantle flow, crustal dynamics and magma genesis associated with slab roll-back and tearing: the eastern Mediterranean case. *Earth Planet. Sci. Lett.* 442, 93–107.
- Molnar, P., Gray, D., 1979. Subduction of continental lithosphere: some constraints and uncertainties. *Geology* 7, 58–62. [http://dx.doi.org/10.1130/0091-7613\(1979\)7<58:SOCLSC>2.0.CO;2](http://dx.doi.org/10.1130/0091-7613(1979)7<58:SOCLSC>2.0.CO;2).
- Moresi, L., Betts, P.G., Miller, M.S., Cayley, R.A., 2014. Dynamics of continental accretion. *Nature* 508, 245.
- Negredo, A.M., Replumaz, A., Villaseñor, A., Guillot, S., 2007. Modeling the evolution of continental subduction processes in the Pamir-Hindu Kush region. *Earth Planet. Sci. Lett.* 259, 212–225. <http://dx.doi.org/10.1016/j.epsl.2007.04.043>.
- Pusok, A., Kaus, B.J., 2015. Development of topography in 3-D continental-collision models. *Geochem. Geophys. Geosyst.* 16, 1378–1400. <http://dx.doi.org/10.1002/2015GC005732>.
- Replumaz, A., Funicello, F., Reitano, R., Faccenna, C., Balon, M., 2016. Asian collisional subduction: a key process driving formation of the Tibetan Plateau. *Geology* 44, 943–946. <http://dx.doi.org/10.1130/G38276.1>.
- Robinson, A.C., Yin, A., Manning, C.E., Harrison, T.M., Zhang, S.H., Wang, X.F., 2004. Tectonic evolution of the northeastern Pamir: constraints from the northern portion of the Cenozoic Kongur Shan extensional system, western China. *Geol. Soc. Am. Bull.* 116, 953–973. <http://dx.doi.org/10.1130/B25375.1>.
- Robinson, A.C., Yin, A., Manning, C.E., Harrison, T.M., Zhang, S.H., Wang, X.F., 2007. Cenozoic evolution of the eastern Pamir: implications for strain-accommodation mechanisms at the western end of the Himalayan-Tibetan orogen. *Geol. Soc. Am. Bull.* 119, 882–896. <http://dx.doi.org/10.1130/B25981.1>.
- Rutte, D., Lothar, R., Schneider, S., Stübner, K., Stearns, M.A., Gulzar, M.A., Hacker, B.R., 2017. Building the Pamir-Tibet Plateau—crustal stacking, extensional collapse, and lateral extrusion in the Central Pamir: 1. Geometry and kinematics. *Tectonics*. <http://dx.doi.org/10.1002/2016TC004294>.
- Schmid, S., Kissling, E., 2000. The arc of the western Alps in the light of geophysical data on deep crustal structure. *Tectonics* 19, 62–85.
- Schneider, F.M., Yuan, X., Schurr, B., Mechie, J., Sippl, C., Haberland, C., Minaev, V., Oimahmadov, I., Gadoev, M., Radjabov, N., 2013. Seismic imaging of subducting continental lower crust beneath the Pamir. *Earth Planet. Sci. Lett.* 375, 101–112. <http://dx.doi.org/10.1016/j.epsl.2013.05.015>.
- Schurr, B., Ratschbacher, L., Sippl, C., Gloaguen, R., Yuan, X., Mechie, J., 2014. Seismotectonics of the Pamir. *Tectonics* 33, 1501–1518. <http://dx.doi.org/10.1002/2014TC003576>.
- Sippl, C., Schurr, B., Yuan, X., Mechie, J., Schneider, F.M., Gadoev, M., Orunbaev, S., Oimahmadov, I., Haberland, C., Abdybaev, U., 2013. Geometry of the Pamir-Hindu Kush intermediate-depth earthquake zone from local seismic data. *J. Geophys. Res.* 118, 1438–1457. <http://dx.doi.org/10.1002/jgrb.50128>.
- Sobel, E.R., Dumitru, T.A., 1997. Thrusting and exhumation around the margins of the western Tarim basin during the India-Asia collision. *J. Geophys. Res.* 102, 5043–5063. <http://dx.doi.org/10.1029/96JB03267>.
- Sobel, E.R., Chen, J., Schoenbohm, L.M., Thiede, R., Stockli, D.F., Sudo, M., Strecker, M.R., 2013. Oceanic-style subduction controls late Cenozoic deformation of the Northern Pamir orogen. *Earth Planet. Sci. Lett.* 363, 204–218. <http://dx.doi.org/10.1016/j.epsl.2012.12.009>.
- Stübner, K., Ratschbacher, L., Rutte, D., Stanek, K., Minaev, V., Wiesinger, M., Gloaguen, R., 2013. The giant Shakh-dara migmatitic gneiss dome, Pamir, India-Asia collision zone: 1. Geometry and kinematics. *Tectonics* 32, 948–979.
- Tapponnier, P., Zhiqin, X., Roger, F., Meyer, B., Arnaud, N., Wittlinger, G., Jingsui, Y., 2001. Oblique stepwise rise and growth of the Tibet Plateau. *Science* 294, 1671–1677. <http://dx.doi.org/10.1126/science.105978>.
- Thielmann, M., Kaus, B.J., 2012. Shear heating induced lithospheric-scale localization: does it result in subduction? *Earth Planet. Sci. Lett.* 359, 1–13. <http://dx.doi.org/10.1016/j.epsl.2012.10.002>.
- Thielmann, M., Rozel, A., Kaus, B.J., Ricard, Y., 2015. Intermediate-depth earthquake generation and shear zone formation caused by grain size reduction and shear heating. *Geology* 43, 791–794. <http://dx.doi.org/10.1130/G36864.1>.
- Tympel, J., 2015. *Numerical Modeling of the Cenozoic Pamir-Tien Shan Orogeny*. Ph.D. thesis. Universität Potsdam, Potsdam.
- van Hunen, J., Allen, M.B., 2011. Continental collision and slab break-off: a comparison of 3-d numerical models with observations. *Earth Planet. Sci. Lett.* 302, 27–37. <http://dx.doi.org/10.1016/j.epsl.2010.11.035>.
- Vogt, K., Gerya, T.V., 2014. From oceanic plateaus to allochthonous terranes: numerical modelling. *Gondwana Res.* 25, 494–508.
- Webb, A.A.G., Guo, H., Clift, P.D., Husson, L., Müller, T., Costantino, D., Yin, A., Xu, Z., Cao, H., Wang, Q., 2017. The Himalaya in 3d: slab dynamics controlled mountain building and monsoon intensification. *Lithosphere* 9, 637–651.
- Yamato, P., Burov, E., Agard, P., Le Pourhiet, L., Jolivet, L., 2008. HP-UHP exhumation during slow continental subduction: self-consistent thermodynamically and

- thermomechanically coupled model with application to the Western Alps. *Earth Planet. Sci. Lett.* 271, 63–74. <http://dx.doi.org/10.1016/j.epsl.2008.03.049>.
- Yin, A., Harrison, T.M., 2000. Geologic evolution of the Himalayan–Tibetan orogen. *Annu. Rev. Earth Planet. Sci.* 28, 211–280. <http://dx.doi.org/10.1146/annurev.earth.28.1.211>.
- Zhao, L., Paul, A., Malusà, M.G., Xu, X., Zheng, T., Solarino, S., Guillot, S., Schwartz, S., Dumont, T., Salimbeni, S., 2016. Continuity of the Alpine slab unraveled by high-resolution P wave tomography. *J. Geophys. Res.* 121, 8720–8737.